Computational modelling of H+-coupled peptide transport via human PEPT1

Megumi Irie[1], Tomohiro Terada[1], Toshiya Katsura[1], Satoshi Matsuoka[2] and Ken-ichi Inui[1]

[1]*Department of Pharmacy, Kyoto University Hospital, Faculty of Medicine, Kyoto University, Kyoto 606-8507, Japan*
[2]*Department of Physiology and Biophysics, Kyoto University Graduate School of Medicine, Kyoto 606-8501, Japan*

H^+-coupled peptide transporter 1 (PEPT1) mediates the transport of small peptides and peptide-like drugs in a pH- and voltage-dependent manner. Here, we investigated the transport mechanisms of PEPT1 for neutral and charged substrates by experimental studies and computational simulation. Uptake studies revealed that the Michaelis-Menten constant (K_m) of glycylsarcosine (Gly-Sar), a neutral substrate, decreased with a fall in pH from 7.4 to 5.5, but at pH 5.0, the K_m increased again. In contrast, the K_m value of an anionic substrate, ceftibuten, declined steadily with decreasing pH. Based on these findings and information from the literature, we hypothesized the transport mechanisms in which (1) H^+ binds to not only the H^+-binding site, but also the substrate-binding site; and (2) H^+ at the substrate-binding site inhibits the interaction of neutral and cationic substrates, but is necessary for that of anionic substrates. To validate these hypotheses, a computational model was constructed and various properties of substrate transport by PEPT1 were simulated. Our model reproduced the voltage dependence, hyperbolic saturation and bell-shaped pH-profile of Gly-Sar transport. Moreover, the various transport properties of negatively and positively charged substrates were also reconstructed. These findings indicated that the inferred mechanisms are able to sufficiently interpret the transport of both neutral and charged substrates by PEPT1.

H^+-coupled peptide transporter 1 (PEPT1) expressed in the brush-border membranes of intestinal epithelial cells mediates the transport of small peptides from the lumen into the cells, and therefore plays an important role in the absorption of protein (Leibach & Ganapathy, 1996; Adibi, 1997; Terada & Inui, 2004). In addition, because of its broad substrate specificity, PEPT1 can accept various pharmacologically active compounds, including β-lactam antibiotics, and serve as an absorptive pathway for these drugs (Inui & Terada, 1999; Daniel & Kottra, 2004; Terada & Inui, 2004). Numerous functional studies have demonstrated that PEPT1 utilizes the H^+ electrochemical gradient as a driving force and exhibits an obvious pH dependence, and that transport by PEPT1 is electrogenic and voltage-dependent regardless of the net charge of the substrate (Fei *et al.* 1994; Mackenzie *et al.* 1996a; Daniel, 2004).

Although the transport characteristics have been delineated, the fundamental transport mechanisms of PEPT1 remain unclear. For example, in the uptake of most neutral substrates, including the typical substrate glycylsarcosine (Gly-Sar), a bell-shaped pH profile with maximal activity at pH 5.5–6.0 is commonly observed (Fei

et al. 1994; Steel *et al.* 1997; Terada *et al.* 1999), but it has not been elucidated why the uptake of these substrates is reduced under more acidic conditions such as at pH 5.0, despite an increase in the H^+ gradient. In addition, the pH profiles of differently charged substrates are distinct from those of neutral substrates (Matsumoto *et al.* 1994; Mackenzie *et al.* 1996a; Wenzel *et al.* 1996; Amasheh *et al.* 1997; Steel *et al.* 1997), the cause of which has not been clarified. Furthermore, it is still controversial how PEPT1 handles differently charged substrates with H^+, including the stoichiometry (Daniel, 2004; Terada & Inui, 2004).

Previously, based on electrophysiological studies, Mackenzie *et al.* (1996b) proposed a kinetic model of Gly-Sar transport by PEPT1. Using the partial reactions of this model, the properties of the pre-steady-state currents induced by PEPT1 in the absence of substrate were well represented (Mackenzie *et al.* 1996b). However, it has not been demonstrated whether the model of Mackenzie *et al.* (1996b) can also display the various features of the steady-state currents evoked by Gly-Sar transport via PEPT1. Furthermore, their model was proposed for Gly-Sar transport only, and therefore it is unclear whether the model can be applied to charged substrates.

Table 1. Equations for the computational simulation of PEPT1 function

$$P(C_o) = \cfrac{1}{\left\{ 1 + \left(\frac{[S_c]_o}{K_{d,Soc1}} \right) + \left(\frac{[H]_o}{K_{d,Ho}} \right) \left(1 + \frac{[S_c]_o}{K_{d,Soc2}} + \frac{[S_n]_o}{K_{d,Son}} \right) + \left(\frac{[H]_{os}}{K_{d,Hos}} \right) \left(\frac{[H]_o}{K_{d,Ho}} \right) \left(1 + \frac{[S_a]_o}{K_{d,Soa}} \right) \right\}} \quad (1)$$

$$P(C_o S_c) = \cfrac{1}{\left\{ 1 + \left(\frac{K_{d,Soc1}}{[S_c]_o} \right) \left[1 + \left(\frac{[H]_o}{K_{d,Ho}} \right) \left[1 + \frac{[S_c]_o}{K_{d,Soc2}} + \frac{[S_n]_o}{K_{d,Son}} + \left(\frac{[H]_{os}}{K_{d,Hos}} \right) \left(1 + \frac{[S_a]_o}{K_{d,Soa}} \right) \right] \right] \right\}} \quad (2)$$

$$P(C_o HS_c) = \cfrac{1}{\left\{ 1 + \left(\frac{K_{d,Soc2}}{[S_c]_o} \right) \left[1 + \frac{[S_n]_o}{K_{d,Son}} + \left(\frac{K_{dHo}}{[H]_o} \right) \left(1 + \frac{[S_n]_o}{K_{d,Soc1}} \right) + \left(\frac{[H]_{os}}{K_{d,Hos}} \right) \left(1 + \frac{[S_a]_o}{K_{d,Soa}} \right) \right] \right\}} \quad (3)$$

$$P(C_o HS_n) = \cfrac{1}{\left\{ 1 + \left(\frac{K_{d,Son}}{[S_n]_o} \right) \left[1 + \frac{[S_c]_o}{K_{d,Soc2}} + \left(\frac{K_{d,Ho}}{[H]_o} \right) \left(1 + \frac{[S_c]_o}{K_{d,Soc1}} \right) + \left(\frac{[H]_{os}}{K_{d,Hos}} \right) \left(1 + \frac{[S_a]_o}{K_{d,Soa}} \right) \right] \right\}} \quad (4)$$

$$P(C_o HHS_a) = \cfrac{1}{\left\{ 1 + \left(\frac{K_{d,Soa}}{[S_a]_o} \right) \left[1 + \left(\frac{K_{d,Hos}}{[H]_{os}} \right) \left[1 + \frac{[S_n]_o}{K_{d,Son}} + \frac{[S_c]_o}{K_{d,Soc2}} + \left(\frac{K_{d,Ho}}{[H]_o} \right) \left(1 + \frac{[S_c]_o}{K_{d,Soc1}} \right) \right] \right] \right\}} \quad (5)$$

$$a = k_1 \cdot P(C_o) + k_3 \cdot P(C_o S_c) + k_5 \cdot P(C_o HS_c) + k_7 \cdot P(C_o HS_n) + k_9 \cdot P(C_o HHS_a) \quad (6)$$

$$b = k_2 \cdot P(C_i) + k_4 \cdot P(C_i S_c) + k_6 \cdot P(C_i HS_c) + k_8 \cdot P(C_i HS_n) + k_{10} \cdot P(C_i HHS_a) \quad (7)$$

$$fluxS = N \left\{ \begin{array}{l} y \left[k_3 \cdot P(C_o S_c) + k_5 \cdot P(C_o HS_c) + k_7 \cdot P(C_o HS_n) + k_9 \cdot P(C_o HHS_a) \right] \\ - (1 - y) \left[k_4 \cdot P(C_i S_c) + k_6 \cdot P(C_i HS_c) + k_8 \cdot P(C_i HS_n) + k_{10} \cdot P(C_i HHS_a) \right] \end{array} \right\} \quad (8)$$

$$fluxH = N \left\{ \begin{array}{l} y \left[k_5 \cdot P(C_o HS_c) + k_7 \cdot P(C_o HS_n) + 2k_9 \cdot P(C_o HHS_a) \right] \\ - (1 - y) \left[k_6 \cdot P(C_i HS_c) + k_8 \cdot P(C_i HS_n) + 2k_{10} \cdot P(C_i HHS_a) \right] \end{array} \right\} \quad (9)$$

$$k_x = \bar{k}_x \exp(-z\gamma VF/2/R/T) \quad (10)$$

$$k_x = \bar{k}_x \exp(z\gamma VF/2/R/T) \quad (11)$$

$$[X]_{eff} = [X]_{sol} \exp(-z\alpha FV/R/T) \quad (12)$$

$$I_{PEPT1} = \sum flux/F/z \quad (13)$$

The equations used for the simulation of the functional properties of PEPT1 are summarized. Five equations (eqns (1–5)) for calculation of the probabilities (P) were derived from the 14-state model shown in Fig. 3A. The representations in the equations and the procedure of simulation using these equations are described in Methods. P(X), the probability of the state X; [X], the concentration of X; C, carrier (PEPT1); H, proton; S, substrate; K_dX, the dissociation constant of X; k_x, the rate constants; the subscripts a, n and c, the charge of substrate (a, anion; n, neutral; c, cation); the subscripts o and i, the facing direction of PEPT1 (o, facing the extracellular side; i, facing the intracellular side).

In the present study, to reveal the transport mechanisms of PEPT1, we first examined the effects of pH on the transport of Gly-Sar and ceftibuten, an oral anionic β-lactam antibiotic, in detail. Based on our experimental results and the previous studies, we hypothesized the transport mechanisms in which (1) H^+ binds not only to the H^+-binding site, but also to the substrate-binding site; and (2) H^+ at the substrate-binding site inhibits the interaction of neutral and cationic substrates, but is necessary for that of anionic substrates. Furthermore, to validate the hypothesized mechanisms, we constructed a computational model, and the transport of neutral and charged substrates by PEPT1 was simulated.

Methods

Cell culture and uptake studies

Caco-2 cells (American Type Culture Collection CRL-1392) were cultured on 12-well cluster plates or 35 mm plastic dishes as previously described (Irie *et al.* 2001), and used on the 14th or 15th day for experiments between passages 33 and 45. Uptake studies using [³H]Gly-Sar (PerkinElmer) and ceftibuten (gift from Shionogi) were performed as previously reported (Matsumoto *et al.* 1994; Terada *et al.* 1999).

Computational modelling of PEPT1

The simulation program was created using Visual Basic.NET. Based on the presumed recognition patterns of PEPT1 for neutral and charged substrates (Fig. 2), we constructed a 14-state model (Fig. 3A). We assumed that H^+ and peptide bindings to PEPT1 are rapid and instantaneously equilibrated. Transitions between PEPT1 facing the extracellular and intracellular sides, denoted as 'o' and 'i', respectively, in Fig. 3A and the equations (Table 1), are reduced to a two-state reaction as described in the Na^+–K^+ pump model (Matsuoka *et al.* 2003). PEPT1 faces the extracellular side in the seven states: empty state (C_o), cationic substrate-bound state ($C_o S_c$), H^+ and cationic substrate-bound state ($C_o HS_c$), H^+ and neutral substrate-bound state ($C_o HS_n$), one H^+-bound state ($C_o H$), two H^+-bound state ($C_o HH$), and two H^+ and anionic substrate-bound state ($C_o HHS_a$). The probabilities (P) of C_o, $C_o S_c$, $C_o HS_c$, $C_o HS_n$, and $C_o HHS_a$ are calculated using eqns (1–5) (Table 1) where P(X) stands for the probability of state X, [X] for the 'effective concentration' of X as described below, and $K_{d,S}$ and $K_{d,H}$ for the dissociation constants of substrates and H^+, respectively. The subscripts c, n and a stand for cationic, neutral and anionic charges of substrates, respectively. $K_{d,Soc1}$ and $K_{d,Soc2}$ are the dissociation constants of

cationic substrates for PEPT1 without or with H^+ at the H^+-binding site, respectively. Because of little information about the efflux properties of PEPT1, we assumed the same mechanism for the intracellular side, and the probabilities of the states facing the interior side were calculated in a similar way as the eqns (1–5) (Table 1). When the 14-state model was condensed into a two-state model (Fig. 3B), the rate constants (a, b) were calculated using the eqns (6) and (7) (Table 1), and then the net fluxes of substrate (fluxS) or H^+ (fluxH) in the time unit were calculated with the probabilities and rate constants (k_{1-10}) using the eqns (8) and (9) (Table 1), in which N stands for the number of PEPT1 proteins.

We assumed that transporters in states C_o and C_i bear one negative charge, and those in C_oHS_n and C_iHS_n are neutral. For S_c carrying one positive charge, we considered that the transporters in C_oHS_c and C_iHS_c have one positive charge, and those in C_oS_c and C_iS_c are neutral. If S_c is a dication, the transporters in C_oHS_c and C_iHS_c bear two positive charges, whereas those in C_oS_c and C_iS_c are monovalent. When S_a has one or two negative charges, we assumed the transporters in C_oHHS_a and C_iHHS_a are neutral and carry one negative charge, respectively. The rate constants (k_{1-10}) were defined based on the Eyring theory of reaction rates (Parent *et al.* 1992b; Mackenzie *et al.* 1996b) as described by the eqns (10) and (11) (Table 1), in which $\bar{k}_x$ stands for the voltage-independent value of k_x, $z(=-1, 0, +1$ or $+2$ in this study) for the net charge which moves with each transmembrane transition, and γ ($= 0.73$) for the fractional dielectric distance. F, V, R and T in the equations have their usual meanings. k_1, k_3, k_5, k_7 and k_9 are described by eqn (10) (Table 1), and k_2, k_4, k_6, k_8 and k_{10} by eqn (11) (Table 1).

The concentrations of ionic species of substrate ($[X]_{sol}$) were obtained using the Henderson-Hasselbalch equation with pK_a values. According to Mackenzie *et al.* (1996b), we assumed a voltage-dependent binding of H^+ and substrate to the outside of PEPT1 ('ion well'). The 'effective concentrations' of charged species and H^+ ($[X]_{eff}$) at the extracellular binding site, the bottom of the 'well', were calculated using eqn (12) (Table 1) (Matsuoka *et al.* 2003). For simplicity, we assumed the same fractional distance for the H^+-binding site and the substrate-binding site. Concerning the fractional distance, $\alpha + \gamma = 1$. For the simulation of electrophysiological studies, the current generated by PEPT1 (I_{PEPT1}) was calculated using the Faraday constant and the net charges which move with transmembrane transition by eqn (13) (Table 1).

Simulation

The steady-state fraction of y in the reduced two-state model was obtained as $y = b/(a + b)$. For the simulation of pre-steady-state currents in the absence of substrate, the differential equation was solved using Euler's method with a time step of 0.05 ms. We obtained almost the same result with a time step of 0.005 ms. The concentrations of ionic species of substrate at different pH values were calculated using pK_a values. In all simulations, the intracellular pH was defined as 7.4.

Results

Studies regarding pH dependence of Gly-Sar and ceftibuten uptake

The pH dependence of 20 μM Gly-Sar transport by PEPT1 exhibited a bell-shaped curve (Fig. 1A). As shown in Fig. 1B, more than 91% of Gly-Sar is neutral at a pH of 5.0–7.4, indicating that the bell-shaped pH profile is attributable to the function of PEPT1, and not to the change in the charge of Gly-Sar. Next, the kinetic parameters (K_m and V_{max}) of Gly-Sar for PEPT1 at various pH values were estimated. The V_{max} value gradually increased as the pH dropped from 7.4 to 5.0, whereas the K_m value decreased markedly with a fall in the pH to 5.5, and when the pH reached 5.0, increased again (Fig. 1C). Previous studies suggested that the coupling ratio of a neutral substrate to H^+ is 1:1, and that the binding of H^+ occurs prior to that of substrate (Fei *et al.* 1994; Mackenzie *et al.* 1996b). According to this, the increase in K_m at alkaline pH is expected, because the proportion of protonated PEPT1 is small and much substrate is necessary to shift the equilibrium of the state of PEPT1 from that having H^+ only to that in which both H^+ and substrate reside. However, this theory cannot explain the increase in K_m at pH 5.0.

For the increase in K_m at acidic pH, we hypothesized that H^+ competes with Gly-Sar at the substrate-binding site, and elevates the K_m value and reduces the uptake. However, this assumption does not apply to anionic substrates such as ceftibuten, because the pH profiles of some anionic substrates do not exhibit a reduction at acidic pH (Matsumoto *et al.* 1994; Wenzel *et al.* 1996). Thus, concerning anionic substrates, we formulated two hypotheses: (1) in contrast to Gly-Sar, the binding of H^+ to the substrate-binding site is necessary for the binding of substrates bearing a negative charge, and therefore competitive inhibition does not occur; (2) besides H^+ at the H^+-binding site, H^+ at the substrate-binding site is cotransported with anionic substrates. These hypotheses were based on previous studies which demonstrated that the transport of negatively charged substrates by PEPT1 evoked inward currents (Mackenzie *et al.* 1996a; Wenzel *et al.* 1996; Steel *et al.* 1997), and that the intracellular acidification accompanied by the transport of anionic substrates was more rapid than that accompanied by the transport of neutral substrates (Steel *et al.* 1997; Kottra *et al.* 2002).

To examine these hypotheses, pH dependence of ceftibuten uptake was investigated. As shown in Fig. 1*D*, the uptake increased sharply as the pH dropped. Within the range of pH used, the principal ionic species was mono- or dianion (Fig. 1*E*), demonstrating that PEPT1 can transport substrates carrying a net negative charge. Moreover, the K_m value of ceftibuten decreased along with the pH, and no increase was observed at the lower pH (Fig. 1*F*). These findings are consistent with the hypotheses stated above.

Construction of transport model for PEPT1

By integrating the findings of the present and previous studies, we constructed a novel model for the transport of H^+ and substrate via PEPT1. Figure 2 is the scheme for the recognition patterns of PEPT1 in terms of charges of substrates. We defined that all substrates share the same substrate-binding site because substrate transport by PEPT1 obeys the Michaelis-Menten equation, and exhibits the competitive inhibition among substrates irrespective
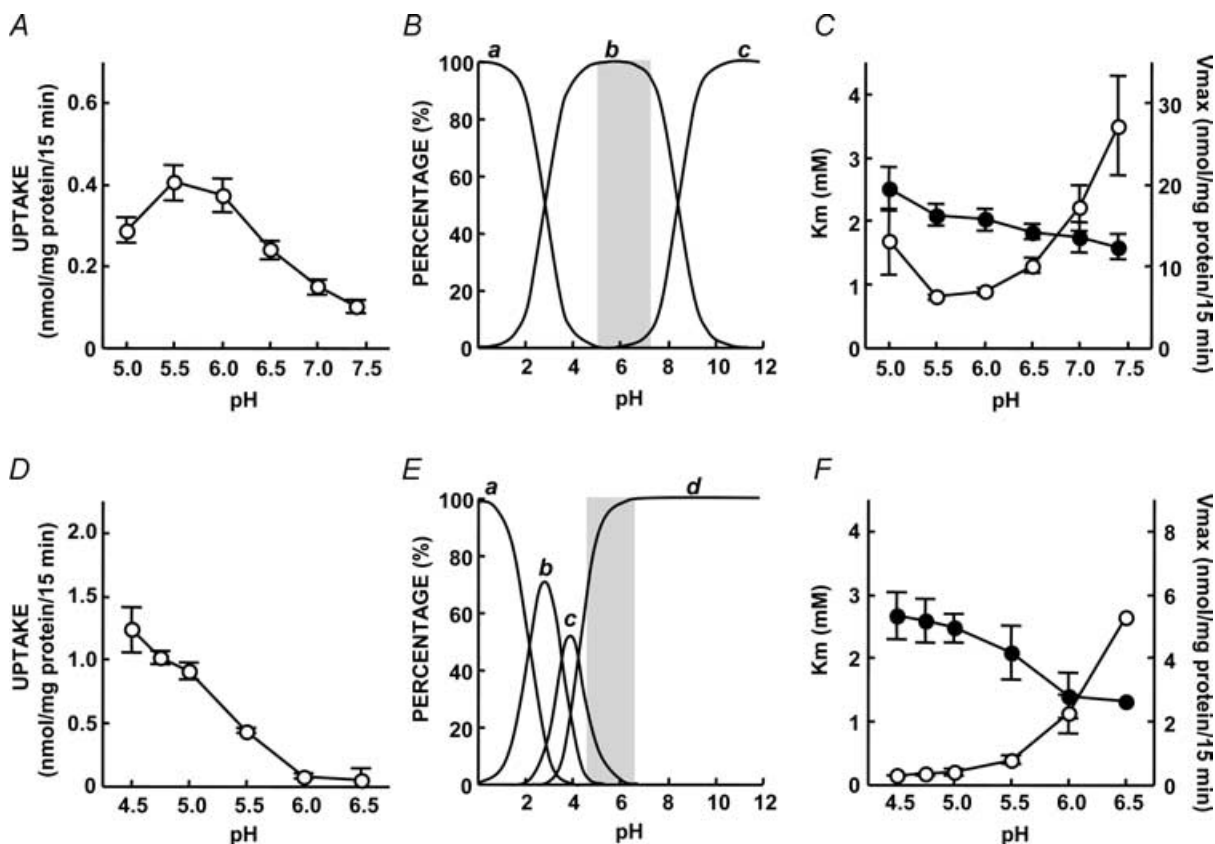

Figure 1. Effects of pH on the charge or uptake of Gly-Sar or ceftibuten

A, pH dependence of [³H]Gly-Sar uptake by PEPT1. The uptake of 20 μM [³H]Gly-Sar from the apical side in Caco-2 cells was measured at various pH values (37°C). Each symbol represents the specific uptake calculated by subtracting the nonspecific uptake from total uptake. The nonspecific uptake was estimated by multiplication of the substrate concentration (20 μM) and the K_d value obtained by the experiments on concentration dependence. *B*, the percentage of ionic species of Gly-Sar as a function of pH. The percentages of monocationic (*a*), neutral (*b*) and monoanionic (*c*) species of Gly-Sar were calculated using the pK_a values (pK_{a1} = 2.83, pK_{a2} = 8.45) by the Henderson-Hasselbalch equation. *C*, pH dependence of the kinetic parameters of [³H]Gly-Sar uptake by PEPT1. The uptake of [³H]Gly-Sar at various concentrations (20–10 000 μM) and pH values (pH 5.0–7.4) was measured at 37°C, and K_m (O) and V_{max} (●) values were estimated using Michaelis-Menten equation. *D*, pH dependence of ceftibuten uptake by PEPT1. The uptake of 50 μM ceftibuten from the apical side in Caco-2 cells was measured at pH 4.5–6.5 by HPLC, and the specific uptake was calculated to be similar to [³H]Gly-Sar. *E*, the percentage of ionic species of ceftibuten as a function of pH. The percentages of monocationic (*a*), neutral (*b*), monoanionic (*c*) and dianionic (*d*) species of ceftibuten were calculated using the pK_a values (pK_{a1} = 2.17, pK_{a2} = 3.67, pK_{a3} = 4.07). *F*, pH dependence of the kinetic parameters of ceftibuten uptake. The uptake of ceftibuten at various concentrations (50–10000 μM) and pH values (pH 4.5–6.5) was measured and K_m (O) and V_{max} (●) values were estimated. *A* and *D*, each symbol represents the mean ± S.E.M. of nine independent monolayers from three separate experiments. *B* and *E*, the shadowed zone represents the range of pH used for the uptake studies. *C* and *F*, the symbols show the means ± S.E.M. of three independent experiments.

of charges (Wenzel *et al.* 1996; Sawada *et al.* 1999), and that empty PEPT1 has one negative charge (Mackenzie *et al.* 1996*b*). It was also defined that PEPT1 has one H^+-binding site to which H^+ is bound prior to substrate, except for the case of cationic substrates (described below). At high pH, as most PEPT1 proteins do not have H^+ at the H^+-binding site (Fig. 2, left), neutral and anionic substrates could not interact. However, we did not exclude the possibility that cationic substrates can interact with empty PEPT1 and be transported without H^+, considering that the intracellular acidification as a consequence of the transport of cationic substrates was moderate (Steel *et al.* 1997; Kottra *et al.* 2002). At moderate pH values, as most PEPT1 proteins have H^+ at the H^+-binding site, both cationic and neutral substrates can be recognized and transported (Fig. 2, middle). As described above, it was assumed that anionic substrates cannot access the substrate-binding site lacking H^+, and that the protonated substrate-binding site can accept only negatively charged substrates (Fig. 2, right). Based on the above hypotheses, a kinetic model for the transport mechanism of PEPT1 was constructed (Fig. 3*A*). To avoid an increase in the number of unknown parameters, the model was made as simple as possible. Next, various simulations were performed to validate this model.

Simulation of the transport of Gly-Sar and ceftibuten

The parameters used for the simulation were described in the legend of Fig. 3, where the values for $\tilde{k}_1$, $\tilde{k}_2$, α and γ were cited from Mackenzie *et al.* (1996*b*). With these four values fixed, other parameters were determined so as to fit the data of Gly-Sar transport (Mackenzie *et al.* 1996*b*). Although other parameter values may be possible, the set of parameters used in this study could reproduce global observations as shown in Figs 4–6, indicating adequacy. In all simulations, the intracellular concentration of

substrate was defined as 0, thus the dissociation constants of substrates at the interior binding site were not determined in this study.

Figure 4 shows the simulation for the electro-physiological studies by Mackenzie *et al.* (1996*b*). The time profiles of the transient charge movements induced by various voltage steps in the absence of substrate were well simulated (Fig. 4*A*), suggesting that our model can quantitatively represent pre-steady-state properties of PEPT1. Furthermore, our model reproduced the inward currents accompanied by Gly-Sar transport, the current–voltage relationship at various concentrations of Gly-Sar (Fig. 4*B*), and voltage dependence of K_m values for Gly-Sar (Fig. 4*C*) and for H^+ (not shown). We then simulated Gly-Sar uptake by Caco-2 cells using a membrane potential fixed at -57 mV, a value that was obtained experimentally (Grasset *et al.* 1984). The saturable uptake conforming to the Michaelis-Menten mode (Fig. 5*A*), the bell-shaped pH profiles (Fig. 5*B*) and the alteration in K_m value by pH (Fig. 5*C*) fitted the experimental data. These findings indicate that the voltage dependence, the concentration dependence and the pH dependence of Gly-Sar transport by PEPT1 can be interpreted by our model.

Next, ceftibuten uptake in Caco-2 cells was simulated using parameters identical to those used for the simulation above, except for the dissociation constants of substrates. As shown in Fig. 5*D–F*, the hyperbolic saturation, pH profiles of the uptake and pH dependence of the kinetic parameters corresponded to the observations, indicating that our model can be applied to anionic substrates.

Simulation of the transport of various charged substrates

Finally, in addition to Gly-Sar, various transport properties of PEPT1 were simulated for charged substrates, anionic
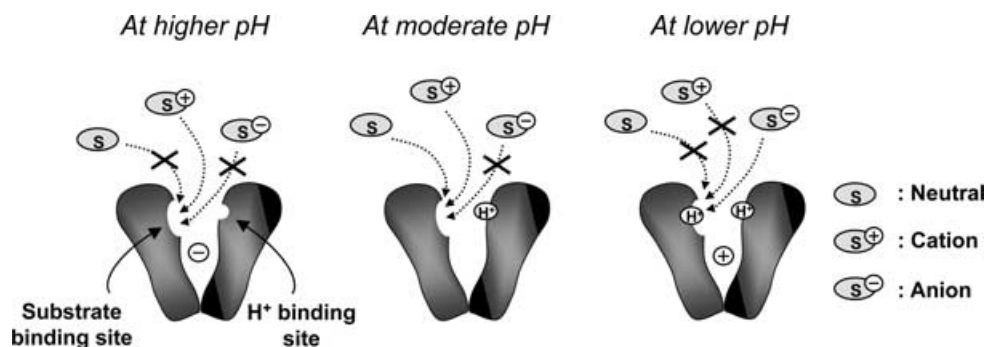

Figure 2. Scheme for the recognition patterns of PEPT1 for neutral and charged substrates
Left, neither neutral substrates nor anionic ones can be recognized by empty PEPT1, which is the principle state at higher pH. Empty PEPT1 can accept only cationic substrates. Middle, at moderate pH, H^+ binds to H^+-binding site, and PEPT1 with H^+ on the H^+-binding site can recognize neutral and cationic substrates, but not anionic ones. Right, anionic substrates can be accepted by only a protonated substrate-binding site at lower pH.

dipeptide Ala-Asp and cationic dipeptides Ala-Lys and Lys-Gly. As shown in Fig. 6*A* and *B*, the inward currents were induced by anionic, neutral and cationic dipeptides over a broad range of membrane potentials, and the K_m value for the cationic dipeptide Lys-Gly exhibited voltage dependence, corresponding to previous reports (Mackenzie *et al.* 1996*a*; Kottra *et al.* 2002). Figure 6*C* shows the simulated pH profiles for Ala-Asp, Ala-Lys and Lys-Gly. Although proper experimental data for Lys-Gly were not obtained, the simulations of the other dipeptides were similar to the observations (Mackenzie *et al.* 1996*a*). Moreover, the transport ratio of H⁺/substrate and the ratio of the total currents induced by the substrate transport to the charge movements by H⁺ flux were calculated (Fig. 6*D*). In contrast to both ratios for Gly-Sar of 1, Ala-Asp was cotransported with more than one H⁺, but the induced current was less than that expected from H⁺ flux. On the other hand, the coupling ratio of Lys-Gly to H⁺ was smaller than 1, and the total current evoked by Lys-Gly was larger.

Discussion

Compared with other symporters, such as Na⁺/glucose cotransporter 1 (Parent *et al.* 1992*a*,*b*), Na⁺/P$_i$ cotransporter 2 (Forster *et al.* 1998) and Na⁺/I⁻ symporter (Eskandari *et al.* 1997), the transport mechanism of PEPT1 has not been clarified. Based on a functional characterization, several studies have proposed the idea for the transport mechanisms of PEPT1 (Mackenzie *et al.* 1996*a*,*b*; Steel *et al.* 1997; Kottra *et al.* 2002), but it has never been examined whether the suggested mechanisms actually describe the transport features of PEPT1. In addition, there is no suggestion for a mechanism which can describe a bell-shaped pH profile of substrate transport via PEPT1. In the present study, by integrating experimental findings with information from the literature, we proposed novel transport mechanisms of PEPT1 applicable to neutral and charged substrates. Furthermore, by computational modelling, we demonstrated that the inferred mechanisms represent global functional features of PEPT1.
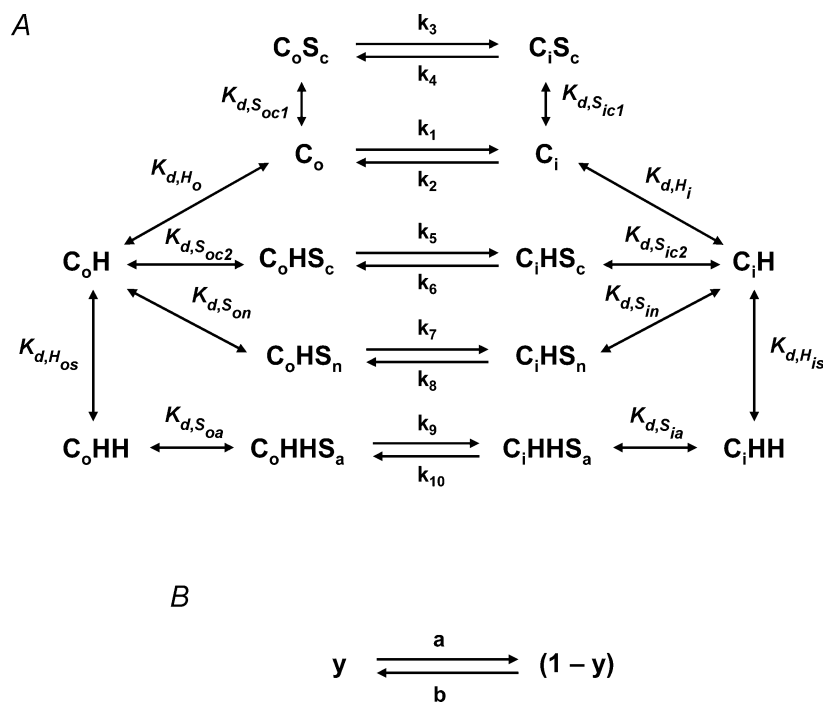

Figure 3. Kinetic transport model of PEPT1
A, the 14-state model for PEPT1. The assumed transport mechanism is represented by a 14-state model as described in Methods. C_o and C_i represent empty PEPT1 facing the exterior and interior sides, respectively, and C_oX and C_iX stand for PEPT1 carrying X. S and H are substrate and H⁺, respectively. $K_{d,X}$ represents the dissociation constant of X, and $K_{d,Ho}$ and $K_{d,Hos}$ stand for the dissociation constants of H⁺ to the H⁺- and substrate-binding sites, respectively. The subscripts a, n and c stand for anionic, neutral and cationic charges of substrates, respectively. The rate constants (k_{1-10}) were calculated using the equations described in the Methods with the following values (per millisecond): $\bar{k}_1 = 0.32$, $\bar{k}_2 = 0.082$, $\bar{k}_3 = 0.6$, $\bar{k}_4 = 0.6$, $\bar{k}_5 = 0.02$, $\bar{k}_6 = 0.02$, $\bar{k}_7 = 0.6$, $\bar{k}_8 = 0.6$, $\bar{k}_9 = 0.2$, $\bar{k}_{10} = 0.2$. The values of $\bar{k}_1$ and $\bar{k}_2$ were cited from Mackenzie *et al.* (1996*b*). The dissociation constants of H⁺ (μM) and fractional distance are as follows: $K_{d,Ho} = 0.45$, $K_{d,Hos} = 17$, $K_{d,Hi} = 0.45$, $K_{d,His} = 17$, $\alpha = 0.27$, $\gamma = 0.73$. These parameters are common to all substrates simulated. *B*, the reduced two-state model for PEPT1. The 14-state model was condensed into a two-state model, which was used for simulation.

pH profiles of substrate transport via PEPT1

The most important mechanism proposed in this study is the binding of H^+ to the substrate-binding site, which is the essential feature different from all previous suggestions Mackenzie *et al.* 1996*a*,*b*; Steel *et al.* 1997; Kottra *et al.* 2002) and provides a possible solution for various pH profiles observed in the transport of substrates with different charges by PEPT1. According to our model, H^+ at the substrate-binding site competitively inhibits the binding of neutral substrates and results in an increase of K_m and a decrease of uptake at acidic pH. On the other hand, as the binding of H^+ to the H^+-binding site shifts the equilibrium from C_o to C_oH, which can accept neutral substrates (Fig. 3*A*), H^+ exerts an inductive effect on Gly-Sar transport. Therefore, the bell-shaped pH profile is the sum of both inductive and inhibitory effects of H^+ on Gly-Sar transport, i.e. the stimulation is predominant at high pH, but at low pH, the H^+-binding site approaches saturation and the excess H^+ occupies the substrate-binding site, and thus the inhibitory effect of H^+ is elicited.

In contrast to neutral substrates, we suggest that H^+ at the substrate-binding site enables negatively charged substrates to interact with PEPT1. As ceftibuten bears a net negative charge at the pH values used (Fig. 1*E*), H^+ does not inhibit but enhances ceftibuten uptake, and the stimulation of uptake with falling pH was more intensive than that of Gly-Sar because of the inductive effects by

two H^+ on both binding sites. In the case of cationic substrates, the effects of H^+ on the substrate transport seem to be more complicated, because the pH profiles of cationic substrates are of variety (Mackenzie *et al.* 1996*a*; Amasheh *et al.* 1997; Guo *et al.* 1999; Kottra *et al.* 2002). Therefore, we hypothesized two mechanisms for the transport of cationic substrates in this model. First, the transport of cationic substrate is affected by H^+ in terms of both induction and inhibition, similar to the case of a neutral substrate (k_5 and k_6 in Fig. 3*A*). Second, the transport of cationic substrate without H^+ is assumed (k_3 and k_4 in Fig. 3*A*), which is inhibited by H^+ on the H^+-binding site because the probability of empty PEPT1 is decreased. Therefore, the effects of H^+ on the transport of cationic substrates are altered by the degree of contribution of two transition steps.

In Fig. 6*C*, pH profiles of both anionic and cationic dipeptides with maximal activity at different pH were shown, which accounted for the mixed effects of various factors, such as the proportion of the ionic charges of substrates, the balances among the dissociation constants of H^+ and substrates. These findings indicate that our model can be applied to differently charged substrates and that the factors described above may be the principal causes determining an apparent pH profile of substrate transport by PEPT1. However, previous studies suggested that the location of charge in the substrate molecule affects the properties of substrate transport (Kottra *et al.* 2002), but
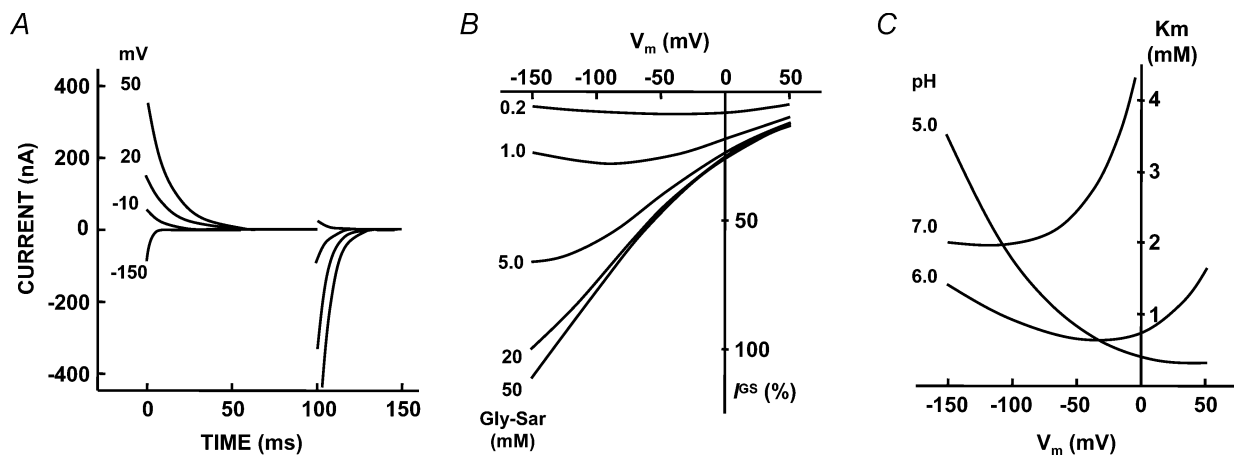

Figure 4. Simulation of electrophysiological properties of PEPT1

A, time profiles of pre-steady state currents by PEPT1. Pre-steady-state currents by PEPT1 in the absence of substrate were simulated using voltage steps from the holding potential (−50 mV) to the indicated potential (−150, −10, 20 or 50 mV) for 100 ms, followed by return of voltage to the holding potential for 50 ms. PEPT1 carrier density and the temperature were assumed as 0.11 pmol per oocyte and 22°C, respectively. *B*, voltage dependence of Gly-Sar-induced currents via PEPT1. Currents evoked by Gly-Sar at various concentrations (0.2–50 mM) were simulated every 0.5 mV under the condition of 22°C, pH 5.0. The magnitude of currents was normalized by that of 20 mM Gly-Sar at −150 mV. *C*, voltage dependence of K_m values of Gly-Sar for PEPT1. Voltage dependence of K_m value for Gly-Sar was simulated. To obtain K_m values, the following calculations were repeated at a membrane voltage of −150 to +50 mV every 0.5 mV at pH 5.0, 6.0 and 7.0. The current of 50 mM Gly-Sar was assumed as I_{max}, and then currents were calculated with increasing concentrations of Gly-Sar from 2 μM with 2 μM increments. The concentration of Gly-Sar that led the current of 50% I_{max} was considered the K_m value. Four dissociation constants of Gly-Sar on the extracellular side ($K_{d,Soc1}$, $K_{d,Soc2}$, $K_{d,Son}$ and $K_{d,Soa}$ in Fig. 3*A*) are defined as 2000 μM.

our model cannot distinguish the differences in chemical structure of substrates. In addition, a valence of net charge of substrate is not considered in this model because of no information. Therefore, there may be substrates for which transport features do not fit the simulation by our model. Further studies concerning structure–activity relationship are necessary to increase the comprehensiveness of the model.

Effects of the membrane potential

As described in Methods, 8 of 10 rate constants and the concentrations of charged molecules were defined as

voltage-dependent. Based on this, the voltage dependence of Gly-Sar transport can be interpreted as follows. Concerning current–voltage (I–V) profiles (Fig. 4B), when the concentration of Gly-Sar was increased, the principal step limiting the rate of the transport cycle shifts from the transition of PEPT1 carrying both H^+ and Gly-Sar (k_7 and k_8 in Fig. 3A) to that of empty PEPT1 (k_1 and k_2), i.e. from the voltage-independent step to the dependent one. Therefore, the currents induced by a higher concentration of Gly-Sar exhibited more intensive voltage dependence. On the other hand, the voltage dependence of K_m value for Gly-Sar seems to be due to two causes: (1) H^+ exhibits the inductive and inhibitory effects, (2) H^+ concentrations
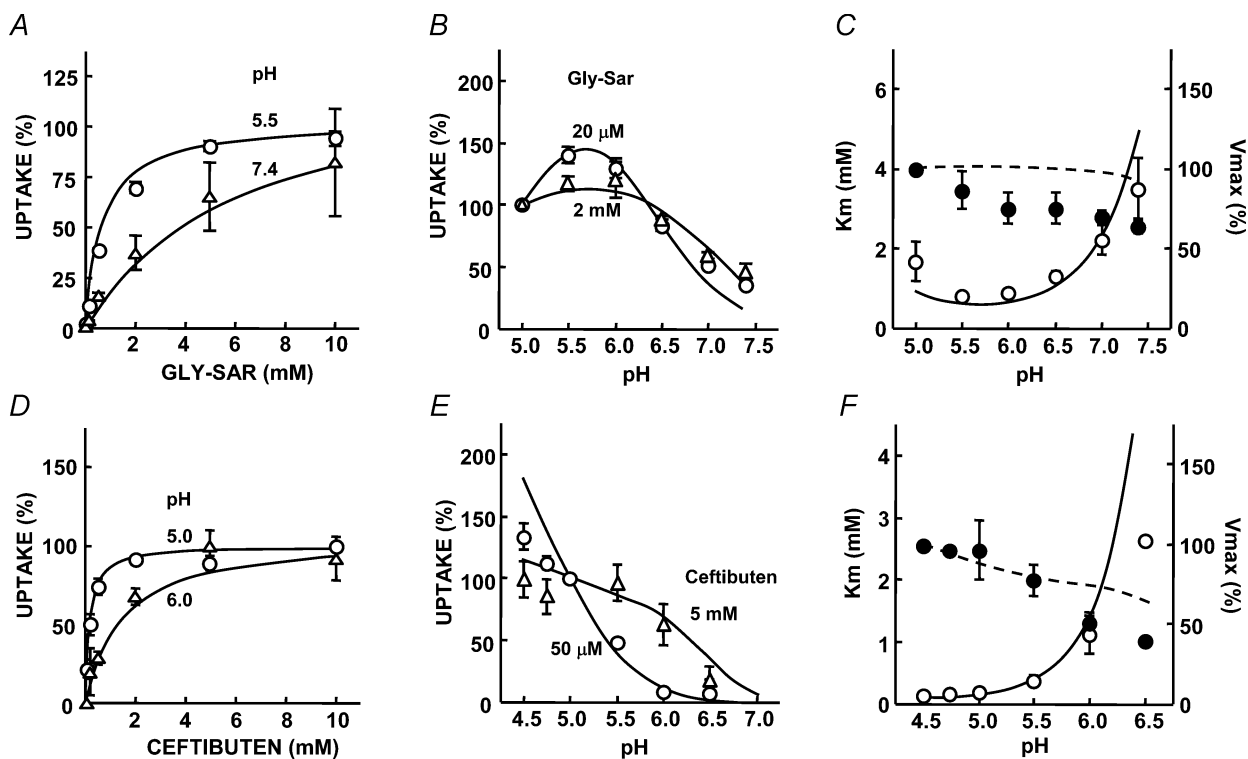

Figure 5. Simulation of Gly-Sar and ceftibuten uptake in Caco-2 cells
A–F, the curves were obtained by simulation at 37°C and −57 mV, and the symbols represent the experimental data. *A*, concentration dependence of Gly-Sar uptake by PEPT1. The transport of Gly-Sar at pH 5.5 and 7.4 was calculated by simulation (curves) at concentrations from 2 μM to 10 mM (every 2 μM). [^{3}H]Gly-Sar uptake at pH 5.5 (○) or pH 7.4 (△) was measured in Caco-2 cells at 37°C, and normalized to the respective V_{max} values. *B*, pH dependence of Gly-Sar transport by PEPT1. pH profiles of Gly-Sar transport were delineated by simulation (curves) at 20 μM and 2 mM Gly-Sar. In simulation, the transport of Gly-Sar was calculated every 0.01 pH unit. 20 μM (○) and 2 mM (△) [^{3}H]Gly-Sar uptake was measured in Caco-2 cells at various pH values. *C*, pH dependence of K_m and V_{max} values for Gly-Sar transport. In simulation, V_{max} (dashed line) was assumed as the transport of 50 mM Gly-Sar, and was normalized to the value at pH 5.0, and K_m values (continuous line) were estimated by calculation of substrate concentration which displayed the transport of 50% V_{max}. K_m (○) and V_{max} (●) values obtained experimentally. *D*, concentration dependence of ceftibuten transport via PEPT1. The transport of ceftibuten at pH 5.0 and 6.0 was simulated (curves) similar to *A*. Ceftibuten uptake was measured at pH 5.0 (○) and 6.0 (△) in Caco-2 cells, and normalized to the respective V_{max} values. *E*, pH profiles of 50 μM and 5 mM ceftibuten transport by PEPT1. The simulation of pH dependence of ceftibuten transport was performed similar to *B* (curves). 50 μM (○) and 5 mM (△) ceftibuten uptake was measured in Caco-2 cells at various pH values. *F*, pH dependence of K_m and V_{max} values for ceftibuten transport by PEPT1. V_{max} (dashed line) was assumed as the uptake of 50 mM ceftibuten, and was normalized to the value at pH 4.5. K_m values (continuous line) were determined similar to *C*. Four dissociation constants of ceftibuten on the exterior side ($K_{d,Soc1}$, $K_{d,Soc2}$, $K_{d,Son}$ and $K_{d,Soa}$ in Fig. 3A) are all 50 μM.

at both H^+- and substrate-binding sites are increased by the negative membrane potential. Thus, the profile of the voltage dependence of K_m value is variable in terms of pH, i.e. at pH 7.0, the inductive effect was well elicited by hyperpolarization, resulting in a decrease of K_m, whereas the inhibitory effect was predominant at pH 5.0 and the K_m value increased.

Compared with other symporters, PEPT1 is ordered to accept diverse physiological substrates, more than 8000 types of di/tripeptides with a variety of charges, and anionic compounds in particular are generally disadvantageous to enter cells because of negative membrane potential. Therefore, protonation of the substrate-binding site may be a distinctive feature for PEPT1 to overcome the difficulty in the transport of anionic substrates. Considering the slightly acidic pH of the small intestine (Adibi, 1997), the protonation of the substrate-binding site seems to be a dexterous strategy to enable the transport of differently charged substrates with high activity.

Stoichiometry

Previous studies demonstrated that not only neutral and cationic substrates, but also anionic substrates, induced inward currents via PEPT1 (Mackenzie *et al.* 1996*a*; Amasheh *et al.* 1997). The following hypotheses about the stoichiometry of anionic substrates have been suggested: (1) before transport, an anionic substrate undergoes protonation, thus the stoichiometry of anionic substrate
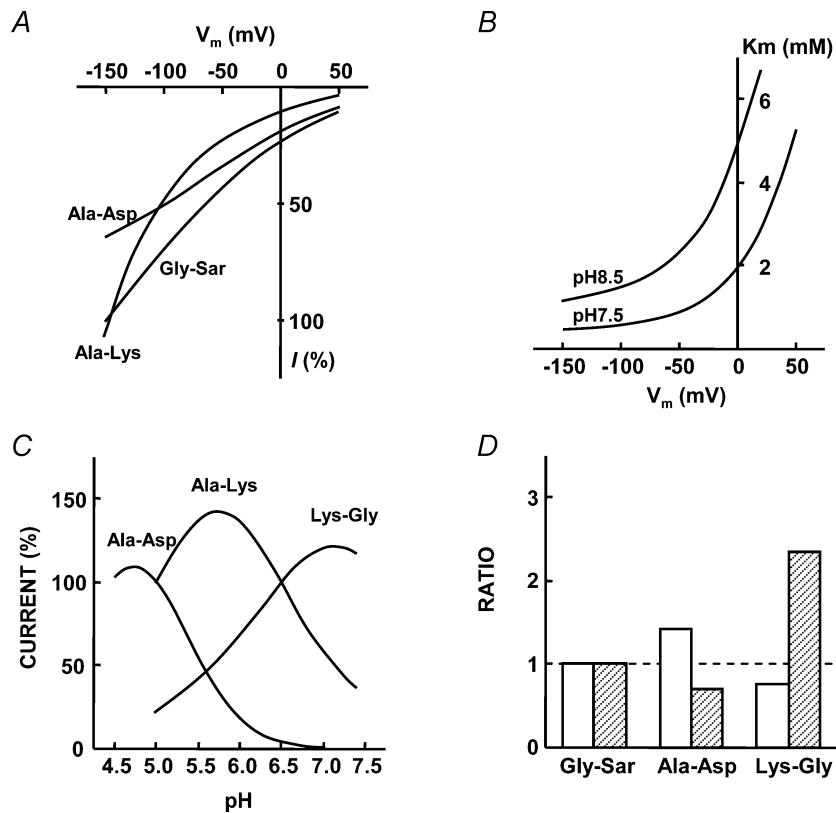

Figure 6. Simulation of the transport properties for various charged substrates

A, current–voltage profiles for neutral and charged substrates. The current–voltage relationship was delineated by simulation for 10 mM Gly-Sar, Ala-Asp and Ala-Lys at pH 6.0, with normalization of each value to that of Gly-Sar at −150 mV. The pK_a values of Ala-Asp (pK_{a1} = 3.0, pK_{a2} = 4.4, pK_{a3} = 8.1) and Ala-Lys (pK_{a1} = 3.2, pK_{a2} = 7.7, pK_{a3} = 10.5) were obtained from a previous study (Mackenzie *et al.* 1996*a*). Four dissociation constants ($K_{d,Soc1}$, $K_{d,Soc2}$, $K_{d,Son}$ and $K_{d,Soa}$ in Fig. 3*A*) of Ala-Asp were 200 μM, and those of Ala-Lys were defined as 1 mM, except for $K_{d,Soc1}$ = 100 mM. *B*, voltage dependence of K_m values for Lys-Gly. Voltage dependence of K_m for Lys-Gly was simulated similar to Fig. 3*C* using pK_a values of Lys-Gly (pK_{a1} = 3.0, pK_{a2} = 8.1, pK_{a3} = 10.7) (Kottra *et al.* 2002) and four dissociation constants defined as 3 mM. *C*, pH dependence of currents evoked by charged substrates via PEPT1. pH profiles of currents induced by Ala-Asp, Ala-Lys and Lys-Gly were simulated similar to Fig. 5*B* at 20 μM, −60 mV. The magnitude of currents was normalized to that at pH 5.0 for Ala-Asp and Ala-Lys, and at pH 6.5 for Lys-Gly. *D*, the transport ratio of H^+ to substrate (open bar) and the ratio of the total currents induced by substrate flux to the charge movement by H^+ flux (hatched bar) were calculated using the simulator at 1 mM substrate concentration, −60 mV and pH 5.0.

to H$^+$ is 1 : 2 (Steel *et al.* 1997; Kottra *et al.* 2002); (2) the transport of an anionic substrate with one H$^+$ is accompanied by a counterflux of a negatively charged ion, which elicits an inward current (Mackenzie *et al.* 1996*a*); and (3) PEPT1 transports only substrate in neutral form (Wenzel *et al.* 1996). However, our studies demonstrated that ceftibuten exists as monoanion or dianion, suggesting that PEPT1 can transport substrates with a negative charge. Although our experimental data can not exclude the possibility of protonation of substrate before permeation via PEPT1 and that of a counterflux of a negatively charged ion, it seems unlikely that protonation of substrate or a counterflux of an anion occurs only in the case of the transport of negatively charged substrate. In the present study, we suggested that the stoichiometry of anionic substrate to H$^+$ is 1 : 2 because of the simultaneous transport of H$^+$ at both H$^+$- and substrate-binding sites. By this model, the inward currents with the transport of Ala-Asp can be obtained (Fig. 6*A*). In addition, the coupling ratio of a neutral substrate to H$^+$ was defined as 1, and that of a cationic substrate as 1 (k_5 and k_6 in Fig. 3*A*) or 0 (k_3 and k_4). The different stoichiometry in terms of the charges of substrates is apparent in Fig. 6*D*. The ratio of H$^+$ to anionic substrate was above 1, but that to cationic one was under 1, and the odd values are as a consequence of the proportion of ionic species. Similarly, the large current of Lys-Gly and the small one of Ala-Asp can be interpreted by the cotransport of H$^+$ and Lys-Gly carrying a positive charge, and the offset of charge movement of H$^+$ by the net negative charge of Ala-Asp, respectively. These results are consistent with previous studies demonstrating that currents evoked by cationic substrates were greater and that the intracellular acidification by basic and acidic dipeptides was more moderate and rapid than that by neutral ones, respectively (Steel *et al.* 1997; Kottra *et al.* 2002).

Our proposed mechanisms, such as the binding of H$^+$ to the substrate-binding site, are not completely proved by experiments, but previous studies demonstrated that the histidine residue in the transmembrane domain of PEPT1 is involved in the substrate-binding site (Terada *et al.* 1996, 1998; Chen *et al.* 2000), which may support the protonation of substrate-binding site. Crystallization of PEPT1 protein may be the promising strategy to evaluate our suggested transport mechanisms of PEPT1.

In conclusion, based on experiments and information from the literature, we proposed the binding of H$^+$ to the substrate-binding site and constructed a transport model of PEPT1 for neutral and charged substrates. Computational simulation reproduced well the concentration-, pH- and voltage-dependent transport of Gly-Sar and pre-steady-state currents by PEPT1. Moreover, various transport properties of negatively and positively charged substrates could be obtained. These findings indicate the possibility of the proposed transport mechanisms of PEPT1, and suggest that computational modelling is a useful strategy to validate the mechanisms presumed.

References

Adibi SA (1997). The oligopeptide transporter (Pept-1) in human intestine: biology and function. *Gastroenterology* **113**, 332–340.

Amasheh S, Wenzel U, Boll M, Dorn D, Weber W-M, Clauss W & Daniel H (1997). Transport of charged dipeptides by the intestinal H$^+$/peptide symporter PepT1 expressed in *Xenopus laevis* oocytes. *J Membr Biol* **155**, 247–256.

Chen X-Z, Steel A & Hediger MA (2000). Functional roles of histidine and tyrosine residues in the H$^+$-peptide transporter PepT1. *Biochem Biophys Res Commun* **272**, 726–730.

Daniel H (2004). Molecular and integrative physiology of intestinal peptide transport. *Annu Rev Physiol* **66**, 361–384.

Daniel H & Kottra G (2004). The proton oligopeptide cotransporter family SLC15 in physiology and pharmacology. *Pflugers Arch* **447**, 610–618.

Eskandari S, Loo DDF, Dai G, Levy O, Wright EM & Carrasco N (1997). Thyroid Na$^+$/I$^-$ symporter. Mechanism, stoichiometry, and specificity. *J Biol Chem* **272**, 27230–27238.

Fei Y-J, Kanai Y, Nussberger S, Ganapathy V, Leibach FH, Romero MF, Singh SK, Boron WF & Hediger MA (1994). Expression cloning of a mammalian proton-coupled oligopeptide transporter. *Nature* **368**, 563–566.

Forster I, Hernando N, Biber J & Murer H (1998). The voltage dependence of a cloned mammalian renal type II Na$^+$/P$_i$ cotransporter (NaP$_i$-2). *J General Physiol* **112**, 1–18.

Grasset E, Pinto M, Dussaulx E, Zweibaum A & Desjeux J-F (1984). Epithelial properties of human colonic carcinoma cell line Caco-2: electrical parameters. *Am J Physiol Cell Physiol* **247**, C260–C267.

Guo A, Hu P, Balimane PV, Leibach FH & Sinko PJ (1999). Interactions of a nonpeptidic drug, valacyclovir, with the human intestinal peptide transporter (hPEPT1) expressed in a mammalian cell line. *J Pharmacol Exp Ther* **289**, 448–454.

Inui K & Terada T (1999). Dipeptide transporters. In *Membrane Transporters as Drug Targets*, ed. Amidon GL & Sadée W, pp. 269–288. Kluwer Academic/Plenum Publishers, New York.

Irie M, Terada T, Sawada K, Saito H & Inui K (2001). Recognition and transport characteristics of nonpeptidic compounds by basolateral peptide transporter in Caco-2 cells. *J Pharmacol Exp Ther* **298**, 711–717.

Kottra G, Stamfort A & Daniel H (2002). PEPT1 as a paradigm for membrane carriers that mediate electrogenic bidirectional transport of anionic, cationic, and neutral substrates. *J Biol Chem* **277**, 32683–32691.

Leibach FH & Ganapathy V (1996). Peptide transporters in the intestine and the kidney. *Annu Rev Nutr* **16**, 99–119.

Mackenzie B, Fei Y-J, Ganapathy V & Leibach FH (1996*a*). The human intestinal H$^+$/oligopeptide cotransporter hPEPT1 transports differently-charged dipeptides with identical electrogenic properties. *Biochim Biophys Acta* **1284**, 125–128.

Mackenzie B, Loo DDF, Fei Y-J, Liu W, Ganapathy V, Leibach FH & Wright EM (1996*b*). Mechanisms of the human intestinal H^+-coupled oligopeptide transporter hPEPT1. *J Biol Chem* **271**, 5430–5437.

Matsumoto S, Saito H & Inui K (1994). Transcellular transport of oral cephalosporins in human intestinal epithelial cells, Caco-2: interaction with dipeptide transport systems in apical and basolateral membranes. *J Pharmacol Exp Ther* **270**, 498–504.

Matsuoka S, Sarai N, Kuratomi S, Ono K & Noma A (2003). Role of individual ionic current systems in ventricular cells hypothesized by a model study. *Jpn J Physiol* **53**, 105–123.

Parent L, Supplisson S, Loo DDF & Wright EM (1992*a*). Electrogenic properties of the cloned Na^+/glucose cotransporter. I. Voltage-clamp studies. *J Membr Biol* **125**, 49–62.

Parent L, Supplisson S, Loo DDF & Wright EM (1992*b*). Electrogenic properties of the cloned Na^+/glucose cotransporter: II. A transport model under nonrapid equilibrium conditions. *J Membr Biol* **125**, 63–79.

Sawada K, Terada T, Saito H, Hashimoto Y & Inui KI (1999). Recognition of 1-amino acid ester compounds by rat peptide transporters PEPT1 and PEPT2. *J Pharmacol Exp Ther* **291**, 705–709.

Steel A, Nussberger S, Romero MF, Boron WF, Boyd CAR & Hediger MA (1997). Stoichiometry and pH dependence of the rabbit proton-dependent oligopeptide transporter PepT1. *J Physiol* **498**, 563–569.

Terada T & Inui K (2004). Peptide transporters: structure, function, regulation and application for drug delivery. *Curr Drug Metab* **5**, 85–94.

Terada T, Saito H & Inui K (1998). Interaction of β-lactam antibiotics with histidine residue of rat H^+/peptide cotransporters, PEPT1 and PEPT2. *J Biol Chem* **273**, 5582–5585.

Terada T, Saito H, Mukai M & Inui K (1996). Identification of the histidine residues involved in substrate recognition by a rat H^+/peptide cotransporter, PEPT1. *FEBS Lett* **394**, 196–200.

Terada T, Sawada K, Saito H, Hashimoto Y & Inui K (1999). Functional characteristics of basolateral peptide transporter in the human intestinal cell line Caco-2. *Am J Physiol Gastrointest Liver Physiol* **276**, G1435–1441.

Wenzel U, Gebert I, Weintraut H, Weber W-M, Clauß W & Daniel H (1996). Transport characteristics of differently charged cephalosporin antibiotics in oocytes expressing the cloned intestinal peptide transporter PepT1 and in human intestinal Caco-2 cells. *J Pharmacol Exp Ther* **277**, 831–839.

Acknowledgements